Piezoelectric small scale generator: towards near-Joule output energy generation

Gael Sebald, Nguyen Thanh Tung, Gaspard Taxil, B Ducharne, Jhordan Chavez, Takahito Ono, Hiroki Kuwano, Elie Lefeuvre, Mickael Lallart

Piezoelectric small scale generator: towards near-Joule output energy generation

Gael Sebald[1*], Nguyen Thanh Tung[1], Gaspard Taxil[1,2], Benjamin Ducharne[1], Jhordan Chavez[2,3], Takahito Ono[4,5], Hiroki Kuwano[1,6,7], Elie Lefeuvre[3], Mickael Lallart[2].

[1]ELyTMaX IRL3757, CNRS, Univ Lyon, INSA Lyon, Centrale Lyon, Université Claude Bernard Lyon 1, Tohoku University, Sendai, Japan
[2]Univ. Lyon, INSA-Lyon, LGEF EA682, F-69621, France·
[3]Centre for Nanoscience and Nanotechnology, University of Paris-Saclay - CNRS, Palaiseau, France
[4] Department of Mechanical Systems Engineering, Tohoku University, Sendai, Japan
[5]Micro System Integration Center, Tohoku University, Sendai, Japan
[6] New Industry Creation Hatchery Center (NICHe), Tohoku University, 6-6-10 Aramaki-Aoba, Aoba-ku Sendai, Miyagi 980-8579, Japan
[7]Sendai Smart Machines Co., Ltd. (SSM), 6-6-40 Aza-Aoba, Aramaki, Aoba-ku, Sendai, Miyagi 980-8579, Japan
E-mail: gael.sebald@insa-lyon.fr

Received xxxxxx
Accepted for publication xxxxxx
Published xxxxxx

Abstract

Research on piezoelectric energy microgenerators from vibrations led to an abundant literature, with various strategies to optimize the frequency range and output power. In contrast, for very low frequency range (<10Hz) and/or for non harmonic mechanical source, the large majority of the strategies are not adapted. This work deals with a small scale piezoelectric generator where the input mechanical source consists of a single force application in the range of hundreds of Newtons (i.e., typical human weight). Contrary to vibrational mechanical sources, such an application context necessitates harvesting as much as energy as possible in a single cycle. This was achieved by assembling several piezoelectric stacks within a mechanical amplification system, and to use the electric field and stress levels close to the limits of the piezoelectric elements. Ericsson cycle (i.e. thermodynamic cycle comprising two iso-electric field and two iso-stress steps) was applied to the piezoelectric material and later using two device prototypes in order to quantify the harvesting capabilities. Finally, in a realistic application point of view, a passive electrical interface based on Bennet's doubler was implemented and compared to the Ericsson cycles in terms of output energy. This electrical energy management strategy successfully allowed working at ultra high electrical field (>2kV/mm) enabling a converted energy density close to the ultimate value. An maximal energy density of 320 mJ/cm^3 was reached using Ericsson cycles, and 130 mJ/cm^3 using Bennet's doubler (~40% of the ultimate energy density). The device comprising ~2.4 cm^3 of piezoelectric material, the net output energy converted and stored per cycle reached 320 mJ. Still, the work presented here can be adapted to other range of forces and displacements for maximizing energy harvesting.

Keywords: Piezoelectric, Ericsson cycle, energy density, compressive stress, energy harvesting, ferroelectric, piezoelectric stack, mechanical amplification, microgenerator

1. Introduction

Piezoelectric materials can be used for mechanical energy conversion into electrical energy, putting them at the heart of energy harvesting from small yet ubiquitous energy sources [1,2]. Vibrations attracted a lot of attention as it was perceived as a source being available in many situations while being of medium energy range (i.e., much larger than radiofrequency waves albeit lower than direct solar light). Most of the works focused on resonant energy harvesters tuned to the input vibration frequency spectrum [3,4]. Various materials and geometries were considered for piezoelectric microgenerator design, as well as application fields like energy harvesting from wind, human body and transportation [5,6], with output power mostly from the µW to mW range. From the state of the art, the comparison of piezoelectric energy microgenerators can hardly draw clear directions for further improvements in the light of the very different mechanical sources in terms of frequency, amplitude and coupling with the energy converter as well as diverse application environments. It was determined that for resonant harvesters, in the case of a imposed input force, the electromechanical coupling factor k^2 and the mechanical quality factor Q_m play key roles. When $k^2 Q_m >> \pi$ [3][7], the resulting power reaches an optimum value independent from the piezoelectric material properties.

On the contrary, the case of non-resonant systems attracted much less attention. The challenge is to be able to harvest in each cycle the maximum energy from a given mechanical source, which might find applications for example in roadways [8][9], or pathways [10].

In such a case, the mechanical design of an energy harvesting device should be adapted to the mechanical source, so that the mechanical stress is high enough to convert as much energy as possible. The majority of the proposed systems in the literature are based on cantilever beams with piezoelectric elements working in 31 mode and operating in a linear way. It is effective in terms of force amplification, but the total quantity of piezoelectric materials that can be implemented remains limited. How to implement a few grams of piezoelectric material working at their ultimate energy conversion capability? From the state of the art, several systems offering force amplification for piezoelectric microgenerators working in 33 mode were proposed [11–14], most of them being based on flexure hinges [15,16]. These works solely relied on the linear properties of the piezoelectric material, hence restricting the full use of the transducers. It was however established that the application of Ericsson cycles under high levels close to the limits, yielding nonlinear response of the transducer, might lead to energy densities in the range of 100~240 mJ/cm^3 [17], decades beyond what linear piezoelectric properties could provide.

In this work, it is proposed a force amplification as for previous works, but with the objective of working in the dielectric and mechanical nonlinear regime, in an attempt to unlock ultra-high energy conversion density. An experimental proof of concept is proposed combining (i) a large quantity of piezoelectric elements, (ii) an effective mechanical energy transfer to the piezoelectric elements, and (iii) an electrical energy management strategy able to obtain the highest energy density thermodynamic cycles. Such an approach enabled fully taking advantage of the non-linear regime of piezoelectric transducers, with electric field and mechanical stress close to the limits, yet with reasonable mechanical input. The energy conversion process was based on Ericsson cycles as a first investigation. The Ericsson thermodynamic cycle provided a reference value of the energy conversion capability of the piezoelectric elements. In a second step, a passive electrical interface, inspired by the Bennett doubler, was implemented for performing high density energy harvesting. With realistic application in mind (Ericsson cycle requiring high voltage controllable voltage sources), this passive interface permitted to work completely above the coercive electric field, where ferroelectric losses are reduced, yet producing an especially large energy density per cycle.

The article is organized as following. In section 2 the design of the piezoelectric microgenerator is introduced, assisted by a theoretical model. It is followed in section 3 by the description of the experimental methods detailing the test bench under high electric field and stress. Then the characterization of a piezoelectric stack actuator is described in section 4, including Ericsson thermodynamic cycles in order to assess the ultimate energy harvesting capability under high levels. In section 5 two designs of experimental prototypes are presented and fully tested. Section 6 presents a passive and efficient electrical interface and energy storage stage along with experimental data. The obtained performance is discussed in section 7, followed by a conclusion.

2. Design of the mechanical system and modelling

The mechanical system was intended to convert a given input force into the required mechanical stress on a large number of piezoelectric ceramic plates which concentrate most of the entering mechanical energy. As exposed in the introduction, the total quantity of active material needed to be increased as much as possible, while remaining adapted to a given force in the hundreds of Newton range. In order to reach a stress level in the range of hundreds of MPa (required to obtain a strong depolarization under stress), the cross-sectional area was kept below 1 cm² and a force amplification was designed. A piezoelectric stack was selected as it offers the advantage of having numerous piezoelectric plates connected electrically in parallel and

mechanically in series. As denoted by Xu et al. [16], it also offers the possibility of relevantly exploiting '33' mode instead of '31' mode, leading to a gain of at least 2 in the energy conversion. The mechanical system was composed of a lever system for force amplification, applying the resulting force on one or several lines comprising one or more piezoelectric stacks, as shown in Figure 1a and b. The electrical network equivalent to the mechanical system is given in Figure 1c, and the electrical model of the piezoelectric stack in Figure 1d. In this analysis, the mechanical and dielectric behavior of the piezoelectric element were linearized for the sake of simplicity.

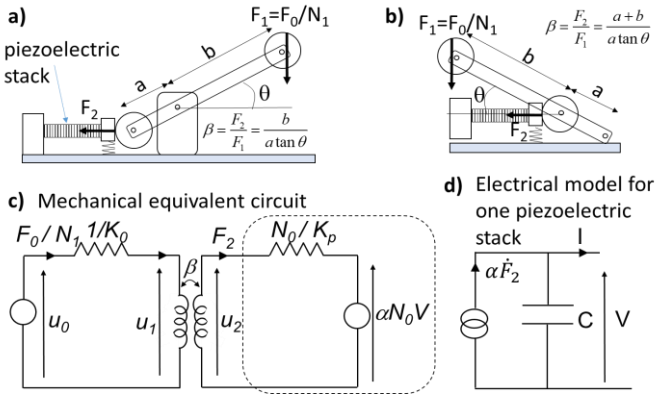

Figure 1: a) Schematic of the mechanical amplification system #1. b) Schematic of the mechanical amplification system #2. c) Electrical network equivalent to the mechanical system. F_0 is the force applied to the whole system comprising N_1 lines of piezoelectric elements after mechanical amplification, F_2 the force applied to each line of N_0 piezoelectric elements. K_0 is an intrinsic stiffness of the lever system, K_p is the stiffness of the piezoelectric stack at constant voltage. β denotes the force mechanical amplification ratio. The term αV is the displacement of the piezoelectric stack when subjected to a voltage V at no stress condition. d) Electrical circuit equivalent to one piezoelectric stack.

The response of the piezoelectric elements is modeled in the case of Ericsson cycle, where the force and the voltage are externally controlled. It consists of charging the piezoelectric element at zero-stress conditions, then applying the stress and inducing a decrease in the polarization. The third step consists of decreasing the voltage at constant stress and finally releasing the stress. The area of the cycle (as shown in the experiment in section 4) corresponds to the converted energy. The piezoelectric stack behavior, taken as a single system, yields the following relationships:

$$I = \dot{Q} = C\dot{V} + \alpha\dot{F}_p \qquad \text{Eq. 1}$$

$$u_p = \frac{F_2}{K_p} + \alpha V \qquad \text{Eq. 2}$$

$$F_2 = F_p \qquad \text{Eq. 3}$$

$$u_2 = N_0 u_p \qquad \text{Eq. 4}$$

where I, Q, V, F_p, u_p, F_2 and u_2 are the electrical current, total electrical charge of one piezoelectric stack, the applied voltage, the force and displacement of one piezoelectric stack and that of the N_0 stacks in series respectively.

The three parameters C (clamped capacitance), α (force factor) and K_p (stiffness), depends on the geometry of the piezoelectric stack and its intrinsic ferroelectric properties. For the capacitance C, each piezoelectric layer of the stack has a thickness of $e_0 = L / N_p$, where L and N_p are the length of the stack and the number of layers respectively; so that the total capacitance of the N_p layers electrically in parallel is given by

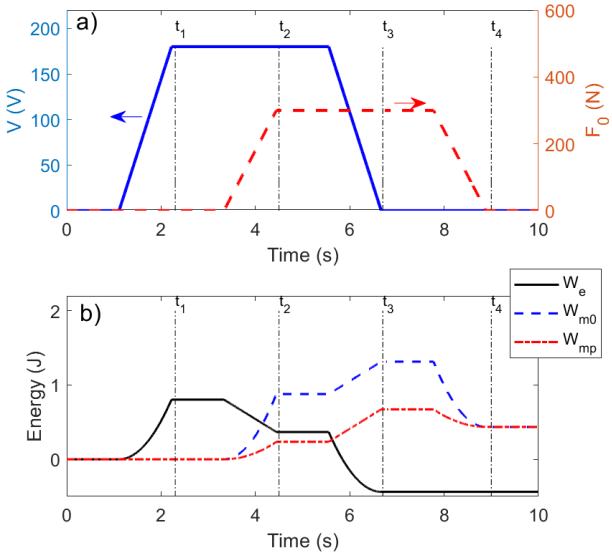

Figure 2: Simulation of energy harvesting using Ericsson cycle from the mechanical system model. a) Typical waveforms for the applied voltage (solid line) and applied external force (dotted line). b) Electrical energy W_e (solid line), mechanical work from external force W_{m0} (dotted line) and mechanical work of the piezoelectric stacks W_{mp} (dash-dotted line). The parameters of the simulation are given in Table 1.

$$C = N_p \frac{\varepsilon_{33}^T A}{e_0} = \frac{\varepsilon_{33}^T A N_p^{\,2}}{L} \qquad \text{Eq. 5}$$

where ε_{33}^T and A are the dielectric permittivity and the cross-sectional area.

$$\alpha = d_{33} N_p \qquad \text{Eq. 6}$$

where d_{33} is the piezoelectric coefficient of the piezoelectric elements

$$K_p = \frac{A}{L s_{33}^E} \qquad \text{Eq. 7}$$

where s_{33}^E is the mechanical compliance of the piezoelectric elements.

It was considered that the external force was applied to N_1 parallel levers each squeezing N_0 piezoelectric stacks in series.

For a given time profile of F_0(t) and V(t), the displacement u_0(t), u_2(t) and the total charge Q_t(t) were computed using the following equations:

$$u_0(t) = F_0(t)\left(\frac{1}{N_1 K_0} + \frac{N_0 \beta^2}{N_1 K_p}\right) + \alpha\beta N_0 V(t) \quad \text{Eq. 8}$$

$$u_2(t) = \frac{N_0 \beta}{K_p} F_0(t) + \alpha N_0 V(t) \quad \text{Eq. 9}$$

$$Q_t(t) = N_0 N_1 Q(t) \quad \text{Eq. 10}$$

where β denotes the force mechanical amplification ratio.

The mechanical work provided by the input force at any time t_0 writes

$$W_{m0}(t_0) = \int_0^{t_0} F_0(t) \frac{\partial u_0(t)}{\partial t} dt \quad \text{Eq. 11}$$

and the total mechanical work of the piezoelectric stacks

$$W_{mp}(t_0) = N_1 \int_0^{t_0} F_2(t) \frac{\partial u_2(t)}{\partial t} dt \quad \text{Eq.12}$$

Finally, the electrical work of the piezoelectric elements was given by:

$$W_e(t_0) = \int_0^{t_0} V(t) I(t) dt \quad \text{Eq. 13}$$

Parameter	Fig. 2	Device #1	Device #2	Optimal
d_{33} (pC/N)	630			
ε_{33}^T (ε_0 F/m)	8500			
s_{33}^E (Pa^{-1})	$2.10\ 10^{-11}$			
A (mm^2)	27.0			
L (mm)	30			
K_p (N/m)	$4.29\ 10^7$			
α (m/V)	$2.70\ 10^{-7}$			
C (F)	$1.24\ 10^{-5}$			
N_1 (#lines)	2	3	1	3
N_0 (#stacks in series)	2	1	3	3
β	15	10	7	16
K_0 (N/m)	$3.5\ 10^4$	$1.9\ 10^4$	$6.1\ 10^4$	$6.1\ 10^4$

Table 1 : Simulation parameters for the illustration Figure 2, and for the two device designs.

Typical signals of simulated Ericsson cycles are displayed in Figure 2a. The four times steps of the Ericsson cycle are indicated in the figure: at time $t=t_1$, the voltage was maximum while the force was at zero. At time $t=t_2$, the force reached its maximum value while the voltage was kept at its maximum value. At time $t=t_3$, the voltage was decreased down to zero keeping the force at its maximum. Finally at time $t=t_4$ both the voltage and force reached zero. When the electric field was applied (from time $t=0$ to $t=t_1$), an increase of the electrical energy was observed, which later decreased as a result of the application of the force between time $t=t_1$ and $t=t_2$, as shown in Figure 2b. The decrease of the electric field between time $t=t_2$ and time $t=t_3$ led to a decrease of the energy to a negative value, in consistence with the energy that flew out from the piezoelectric materials. Between time $t=t_3$ and time $t=t_4$, only the mechanical energy decreases down to the value of the electrical energy (in absolute value), and corresponded to the converted mechanical energy.

The model was later used to simulate the experimental data described in section 5 and to better understand the energy conversion mechanisms and ways to improve it. The determination of the simulation parameters were based on the experimental characterization of the piezoelectric stack. Piezoelectric coefficient d_{33} and dielectric permittivity ε_{33}^T were averaged between 0 and 100 MPa, and between 0 and 2.6 kV/mm. The mechanical compliance was taken at $2.1\ 10^{-11}$ Pa^{-1}, which is a standard value for very soft PZT material. The parameters A, L, K_p, α and C were calculated from the geometry and properties of the piezoelectric material and of the device only. The intrinsic stiffness K_0 was finally determined from the maximum experimental stored elastic energy $W_{m\,max}$.

3. Experimental methods

The piezoelectric materials were first characterized, both for their ferroelectric behavior at no stress and under compressive stress. The test bench consisted of a compression test equipment (Shimadzu AGS-X, Japan) applying a given static force to the piezoelectric material. The sample electrodes were connected to a high voltage amplifier (AIE Inc., Trek 10/10B-HS, USA) delivering a bipolar triangular shape waveform, and driven by a function generator (Tektronix AFG1022, USA). The current was measured with a current amplifier (Stanford research®, USA) connected in series, and exhibiting an input resistance of 1Ω. The polarization was calculated from the time integral of the current. All signals were recorded using a Data Acquisition System (Dewesoft Krypton 8LV, Slovenia), exhibiting an input resistance of 1 MΩ.

The ultimate energy conversion capability of the selected material was determined experimentally by performing Ericsson cycle. Using the same test bench described above, the waveforms were modified in order to have a four step process as in Figure 2a.

In the final experiments, a passive electrical interface based on Bennet's doubler [18] was directly connected to the piezoelectric elements to perform partial Ericsson cycles. In this case, the voltage and current of the piezoelectric elements, and the storage capacitor were monitored.

The prototype was fabricated using customized mechanical parts (levers, rotation and linear guides, hinges…). It was equipped with a displacement sensor (Panasonic HG-C1100-P, Kadoma, Japan) for monitoring the contact frame displacement, and determining the mechanical work of the external mechanical source.

4. Piezoelectric stack characterization

The piezoelectric stack actuator B58004M4030A020 (TDK, Munich, Germany) was selected. Details on the ferroelectric behavior under stress of a similar piezoelectric

stack are given in [19]. It was made of ~430 soft PZT layers of 70 µm thickness separated with electrodes. The total length of the actuator was 30mm, with cross-sectional dimensions 5.2 mm x 5.2 mm.

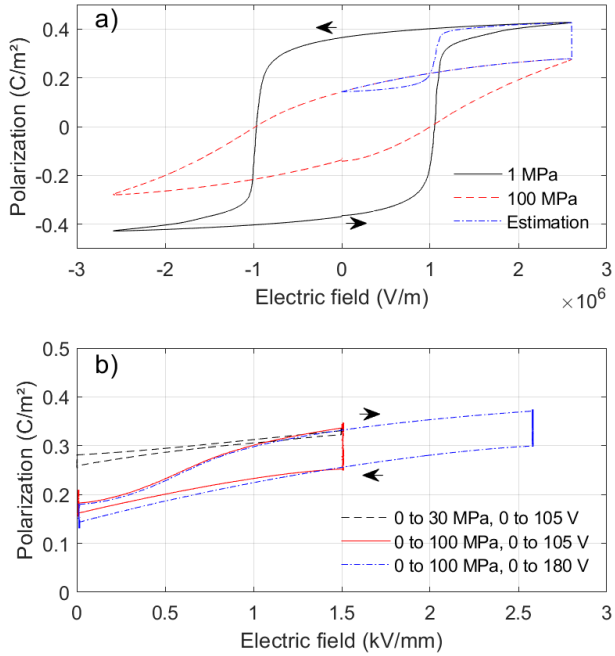

Figure 3: a) Bipolar cycles at 1 MPa and 100 MPa on a piezoelectric stack, with the estimated Ericsson cycle area in blue dotted line. b) Ericsson unipolar cycles on a piezoelectric stack. Counter clockwise cycles corresponded to dissipated energy (i.e. hysteresis losses) and clockwise cycle to energy converted into electrical energy.

Test	Electric field (kV/mm)	Mechanical stress (MPa)	Converted energy density (mJ/cm^3)	Converted energy by the piezoelectric stack (mJ)
#1	1.5	30	13.9	11.3
#2	1.5	100	74.5	60.4
#3	2.6	100	163	132

Table 2: Ericsson cycle energy densities tested on one piezoelectric stack.

The transducer was first characterized under static stress and bipolar voltage excitation. Figure 3a depicts the polarization versus electric field at 1 MPa and under 100 MPa static stress levels. A typical change of the hysteresis cycle shape was obtained, as denoted in other works [20][21]. Based on the bipolar cycles, using the same estimation method as in [17], a maximum energy density conversion of 210 mJ/cm^3 was estimated (cycle delimited by the blue dotted line in Figure 3a). In a second experiment, the Ericsson cycles were tested on the piezoelectric stack actuator with electric field and stress waveforms as in Figure 2a. The stress being high enough to induce irreversible polarization variations, the Ericsson cycles were systematically done three successive times. The 2nd and 3rd attempts were made sure to be similar. The 3rd cycle was then used to determine the converted energy density by using $W_{dens} = \oint EdP$ (enclosed area of the polarization cycle).

The Ericsson cycles were tested under three conditions in terms of mechanical stress and electric field magnitudes. The resulting polarization versus electric field are displayed in Figure 3b. The areas enclosed by the cycles corresponded to the converted energies, which are given in Table 2. The resulting energy densities were consistent with previous works on several ferroelectric materials [17], with typical values for soft PZT ~100 mJ/cm3 under similar stress and electric field conditions as test #2.

5. Practical implementation

From the state of the art, various solutions exist for force amplification. Systems based on flexural hinges require a careful design to reach the objectives in terms of loading capacity, stability of the amplification ratio with the displacement, and control of parasitic motions [14]. In this work, a simpler system was chosen based on a true lever type amplification. This allowed converting a vertical force into a horizontal one along with force amplification ratios from 7 to 10, while being relatively insensitive to the accuracy of the dimensions and positioning. It makes also possible to increase the number of piezoelectric stacks put in series or in parallel, thus increasing the total volume of active material.

For the application device design, a first configuration with a low-angle lever was considered as depicted in Figure 1a and Figure 4a. The angles and lengths were optimized for ensuring a small lever displacement during the force application. The thicknesses of the frame and various holding parts were furthermore larger than 1 cm for avoiding unnecessary bending of the parts, which were made of steel to be stiff enough.

The analysis of the mechanical structure gave a force ratio of $\beta = b/(a\tan\theta)$, where a, b and θ are the short length of the lever (4.8 cm in this study), the long length of the lever (17.6 cm), and its angle (20°) respectively. The device comprised three levers systems, each squeezing a separate piezoelectric stack. The external force was applied to the top metallic plate as shown in Figure 4a. With the selected dimensions, a force ratio of 10 was expected.

In a first experiment, the piezoelectric stacks were replaced by custom force sensors made of aluminum bars equipped with strain gauges, with similar dimensions and Young's modulus as the piezoelectric stacks. When the external force was applied at an equal distance from the contacts points, the force on each lever was measured and showed little discrepancies between each other (<10%). The sum of the three forces was 7300 N for an external force of 700 N, yielding a force ratio of 10.5, close to the expected force ratio of 10.1.

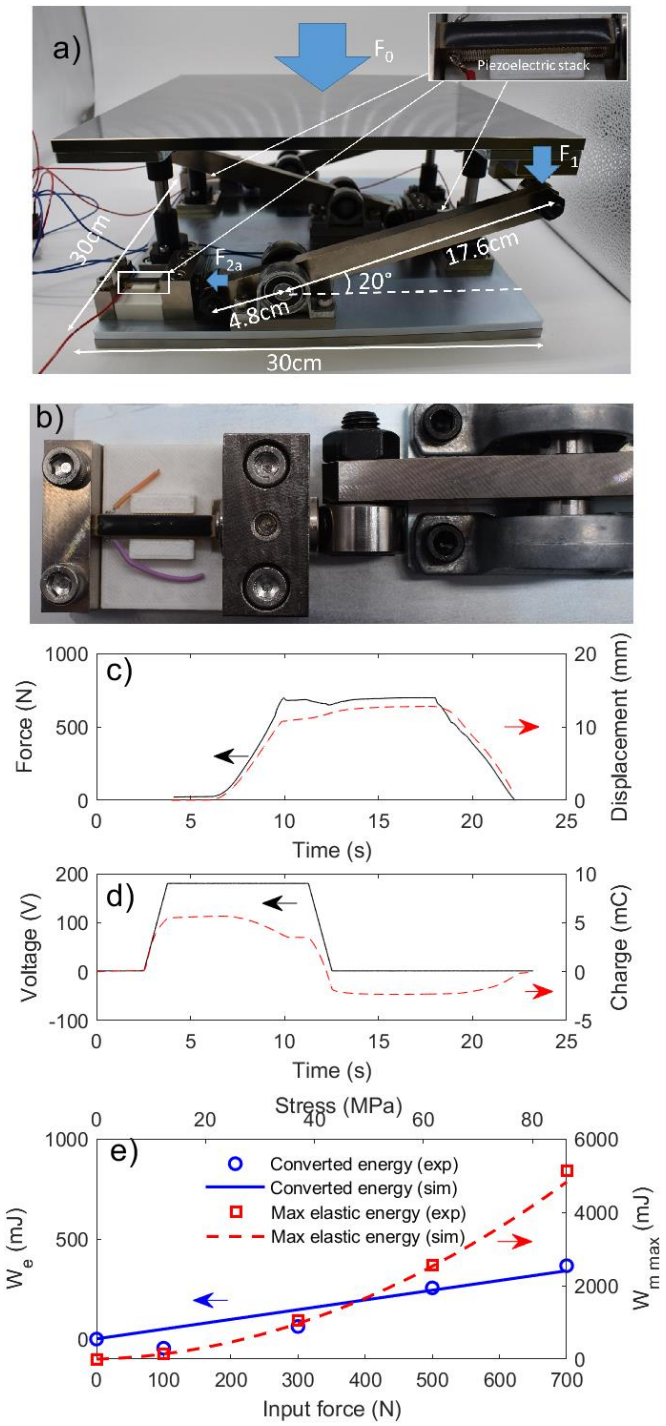

Figure 4 : a) Photograph of device design#1, where the external force is pushing three levers (each one squeezing one piezoelectric stack). b) Enlarged view of the piezoelectric stack and the contact with the lever. c) Waveforms of the imposed force and induced displacement for a 700N mechanical input. d) Waveforms of the imposed voltage and induced charge variation. e) Converted electrical energy by Ericsson cycle and maximum stored elastic energy, versus applied external force. The corresponding stress applied to the piezoelectric materials is indicated on the top horizontal axis.

After replacing the force sensors by piezoelectric stacks, Ericsson cycles were tested for several external force magnitudes. The mechanical work of the external actuator was determined from the external force F_0 and displacement measurements. External forces ranging 100N to 700N were tested, and the resulting net converted energy and maximum elastic energy are given in Figure 4b. The experimental cycles for an external force of 700 N were very close to that in Figure 3b. A net output energy as high as 360 mJ was measured, corresponding to 120 mJ per stack, close to the previous characterization value.

The model parameters given in Table 1 were set as detailed in section 3, and a good agreement with experimental data was observed for both elastic and converted energy (Figure 4b). Some discrepancies were observed regarding the converted electrical energy at 300 N and below, probably because the model did not take into account hysteresis losses that could become higher than converted energy for low force levels. In addition, the piezoelectric effect might show also nonlinearities with the level of the stress as well as the mechanical system.

The maximum stored mechanical energy was considered to be the energy reservoir partially converted into electrical energy. For all tested forces, it appeared that the maximum stored mechanical energy was much larger than the converted energy. The reason lied in the mechanical stiffness of the piezoelectric stacks (K_p/β^2), which was higher than that of the lever system (K_0). Consequently the lever system stored more energy than the piezoelectric stacks. As only the latter one could be converted onto electrical energy, only 7% of the maximum stored mechanical energy could be converted eventually.

With the objective of optimizing the convertible energy over the total stored mechanical energy, the parallel configuration of the three piezoelectric stacks was modified into a series configuration as shown in Figure 1b and picture Figure 5a. This allowed a higher ratio of mechanical energy stored in the piezoelectric transducers compared to the lever system. The mechanical stiffness of the piezoelectric stacks assembly was lowered by a factor of 9, and the lever system stiffness was also slightly increased (fewer parts led to a minimization of the adjustments and gaps responsible for an overall softer spring behavior).

In this second design, the force amplification became $\beta = (a+b)/(a\tan\theta)$. The force amplification factor was experimentally confirmed at a value of 7.

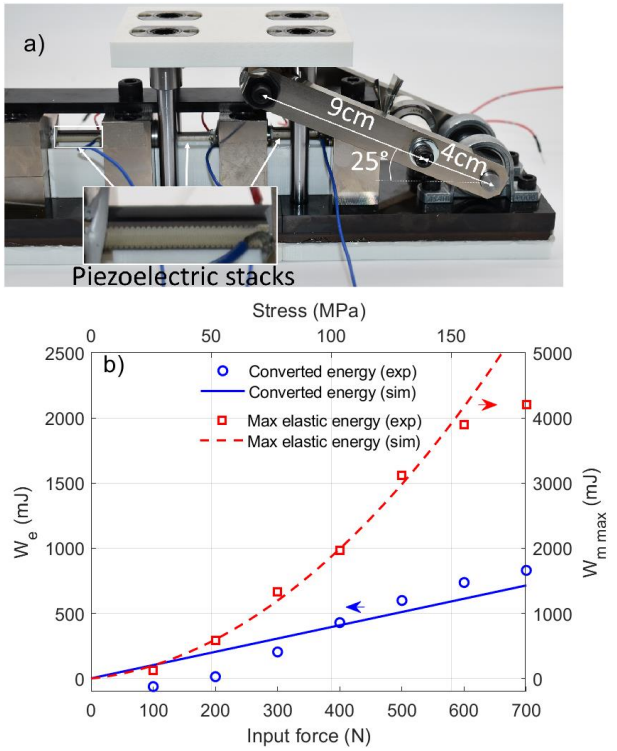

Figure 5 : a) Photograph of device design#2, with piezoelectric stacks mechanically assembled in series. The force is applied vertically on the top white plate, which is converted into a larger horizontal force squeezing the piezoelectric stacks. b) Converted electrical energy and maximum stored elastic energy, versus applied external force.

A photograph of the device is displayed in Figure 5a. The Ericsson cycles were then tested for different input forces ranging from 100 N up to 700 N. The resulting polarization versus electric field cycles were again very similar to the previously obtained ones. The resulting output converted energy and maximum stored elastic energy are given in Figure 5b, along with the simulation from the model. For this design too, the model showed a good accuracy in the computed maximum elastic energy and converted energy. For the highest tested force at 700 N however, the experimental maximum elastic energy showed a lower value compared to the simulation, probably due to a nonlinear behavior of the spring of stiffness K_0. As for the converted energy, we also observed a discrepancy for the low force values, certainly due again to the hysteresis losses that were neglected in the model.

Compared to device design#1, the converted energy density is about twice for the same input force and similar stored elastic energy. It should be noted that this second design allowed to reach a much higher mechanical stress (up to 170 MPa), thus leading to a larger output energy.

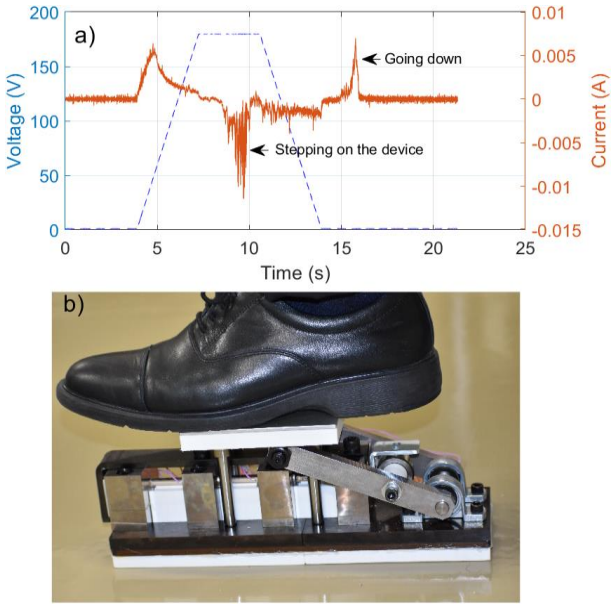

Figure 6 : Testing of the device with a true step. a) Experimental voltage (dashed line) and current (solid line) as a function of time. b) Photograph of the device when stepping on it.

This result highlighted the importance of controlling the parasitic compliance of the mechanical amplification system that should be ideally much stiffer than the piezoelectric elements.

In a second experiment, the force was applied by physically stepping on the upper plateau of the device (white part at the top of Figure 5a). The voltage was controlled externally as for other Ericsson cycle experiments. The exact time profile of the force application was not controlled and was rising faster than that applied with the controlled compression test equipment. The resulting current time profile for a force of 700 N is given in Figure 6a. A photograph of the experiment is given Figure 6b. The current exhibited three distinct peaks: a positive peak when the voltage is increased (charge of the electrical capacitance of the piezoelectric ceramic), a negative peak when applying the force (depolarization due to the mechanical stress and electromechanical conversion through piezoelectric activity), and a negative peak when decreasing the voltage (discharge of the piezoelectric capacitance). With a force of 700 N the output converted energy was experimentally found to reach as high as 776 mJ per step, whereas an energy of 578 mJ was measured for the case of a 500 N force.

6. Electrical interface

All the previously mentioned results dealt with Ericsson cycle whose practical implementation would be delicate as such an approach requires fully controllable voltage source. This may however use excessive energy for standalone operations, thus compromising the energy balance of the global device. In this work a fully functional and realistic (i.e., standalone) prototype was targeted. The main aspects in

selecting the most suitable interface consisted in having a viable a fully passive system, while permitting beneficiating of large energy cycles in the voltage/charge diagram. More specifically, while Ericsson cycles exhibited the highest area for a given maximal voltage (or electric field), another limitation of its realistic implementation is that it led to a significant, if not complete, depolarization. Hence, the cycle should be cropped in order to maintain remnant polarization, leading to pseudo-rectangular cycle. An interface able to combine both a passive approach (i.e., without requiring controllable source) and rectangular cycle lies in a diode-based circuit [22], exposed in Figure 7a. However, in this approach the low voltage source V_L is always providing energy without recovering it, eventually leading to its depletion and thus compromising the viability of the scheme.

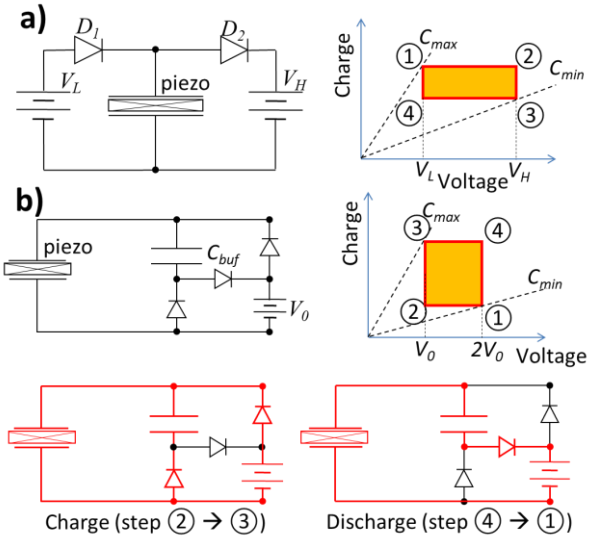

Figure 7 : a) Diode-based electrical interface. b) Bennet's doubler electrical interface and associated cycle, with emphasis on charge and discharge pathes.

Based on these considerations, the selected interface consisted of an electrical version of the Bennet doubler [18], comprising three diodes and two storage capacitors (Figure 7b). In particular, the Bennet's doubler permits, thanks to the successive conductions of the diodes, to operate similarly to the previous architecture, but with only one source that is thus replenished with an energy amount greater than the provided one, ensuring the applicability and viability of the microgenerator. More specifically, the charge is obtained through a parallel configuration of the voltage source and the buffer capacitance, while the discharge (energy harvesting process) yields a series connection of the buffer capacitance and the voltage source, leading to a voltage seen by the transducer being twice as the voltage source value.

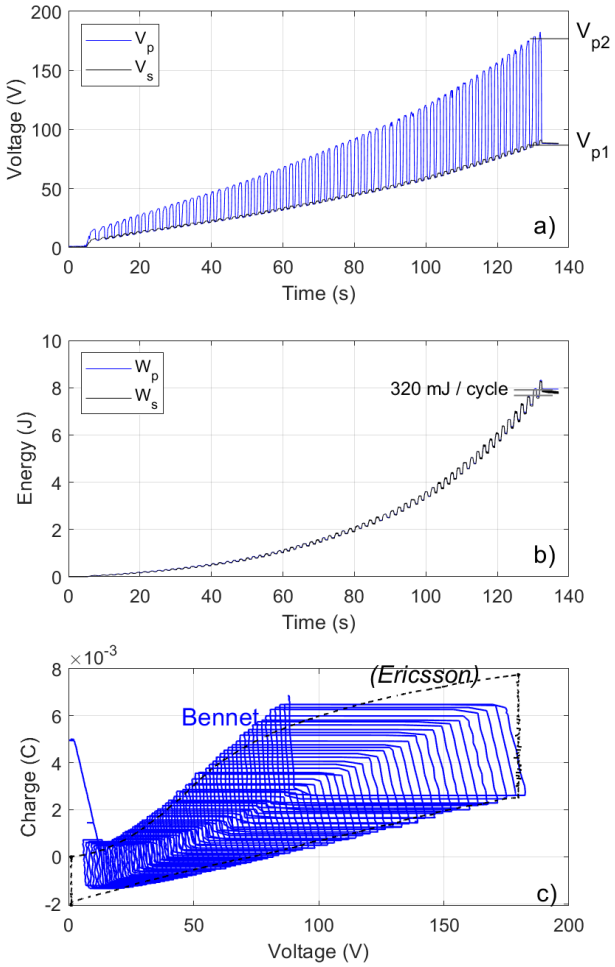

Figure 8 : Test of the fully passive Bennet's doubler interface for energy harvesting from device design#2, under cycles with a force of 700 N. a) Voltage vs. time. b) Converted and stored energy vs. time. c) Charge vs. voltage. Ericsson cycle recalled in dotted lines.

In the present work, an original application of the Bennet's doubler was proposed. As conventional works consider such a circuit for electrostatic device (i.e., based on capacitance variation of the transducer only), this study implemented the circuit using piezoelectric elements, which also allowed generating charges. Such an active transduction system allowed getting rid of any voltage source, and permitted beneficiating of a self-starting system. In this work, the voltage source was replaced by a storage capacitor of 1 mF, leading to a fully passive circuit. Energy cycles spontaneously appeared and charged the storage capacitors, thus inducing further voltage increase and larger cycle's area [23]. Several improvements (e.g., multiple feedback stages) might be possible for adapting the device as close as possible to the exact desired shape of the charge versus voltage behavior, in order to maximize the area enclosed [24].

In our experiment, when the force was applied to the piezoelectric elements from a starting initial voltage V_{p1}, it remained in open circuit condition until the voltage reached a value V_{p2} (twice the starting value), followed by a decreasing

charge at constant voltage. When the force was released, the voltage went down at constant charge until the value reached the low voltage V_{p1}, followed by an increase of the charge back to a value slightly higher than the initial value. The repetition of the cycles led to a gradual increase of the starting voltage V_{p1} and of the area enclosed by this cycle. The piezoelectric stacks were connected in parallel to the interface, and 50 successive steps at 700 N were applied to the device design#2 from a totally discharged state.

Due to the piezoelectric activity of the active elements, the initial voltage increased when applying the force, which initiated the successive and gradual charges of the buffer and storage capacitors. From these measurements, the electrical power was integrated over time to compute the electrical work of the piezoelectric elements $W_p(t_0) = \int_0^{t_0} V_p(t) I(t) dt$. The total stored electrical energy in the capacitors was determined by $W_s(t) = \frac{1}{2}(C_1 + C_2) V_s(t)^2$.

The time signals of the voltages are displayed Figure 8a. The piezoelectric voltage minimum value over one cycle followed as expected that of the storage capacitor and reached twice the value when the force was applied. The energy stored in the piezoelectric materials and in the storage capacitor are displayed in Figure 8b. It was observed a quasi-quadratic increase of the energy with time, suggesting that the highest starting voltage V_{p1} was preferable for increasing the output energy. However, the limit was given by the dielectric strength of the piezoelectric elements, which led to a limit of 180 V on the piezoelectric elements, as recommended by the supplier. Therefore, the cycles were stopped when the voltage reached this limit. For the last cycle, the storage capacitors were therefore charged at 90V, and the voltage of the piezoelectric elements evolved between 90V and 180V. In this case, the energy per cycle reached 320 mJ per cycle. It corresponded to ~40% of the ultimate convertible energy obtained using the active Ericsson cycle.

Interestingly, the shape of the Bennet's doubler cycles (given in Figure 8c) outfitted the shape of the Ericsson cycles. It was first expected that the top-left and bottom-right angles of the Bennet's doubler cycles would belong to the curves obtained during Ericsson cycles measurements, which was not the case in experiments. This phenomenon was interpreted in terms of irreversible depolarization induced by the mechanical stress. When applying the Ericsson cycle, the charging curve started from a zero voltage, and the first part of the curve corresponded to the (re)polarization from a partially depolarized state. In contrast, the Bennet's doubler did not bring the voltage back to zero, so that the depolarization effect was lower, and the equivalent charging branch corresponded to another first-order reversal curve, with a higher polarization value. As a consequence, the cycles induced by the Bennet's doubler were higher than expected, reaching about 40% of that of the Ericsson cycle.

7. Discussion and position with respect to state-of-the-art

Qian et al. [13] proposed a frame amplification system for energy harvesting from human steps. Under 500 N, inducing a displacement of 4 mm peak-to peak, a maximum power of 11 mW at 1 Hz was successfully achieved. Chen et al. [25] proposed also a frame amplification adapted to traffic roads. Under an input step force of 1333 N, and 2.5 mm deflection of the system and an output energy per cycle of 121 mJ was obtained, representing 5.83% of the input mechanical energy. In our work, the force amplification scheme was combined with Ericsson cycles, later simplified using a Bennet's doubler interface, allowing taking advantage of nonlinear dielectric behavior. Although not giving as high energy density as Ericsson cycles, the Bennet doubler allowed reaching almost 40% of the latter, leading to an output energy of 320 mJ per cycle (*i.e.*, 320 mW at 1 Hz), for a force input of 700 N and a peak-to-peak displacement of 12 mm. Compared to [13] and [25], our results showed significantly more output energy and a higher efficiency, thanks to the utilization of the piezoelectric materials in high electric field – and strongly nonlinear – region.

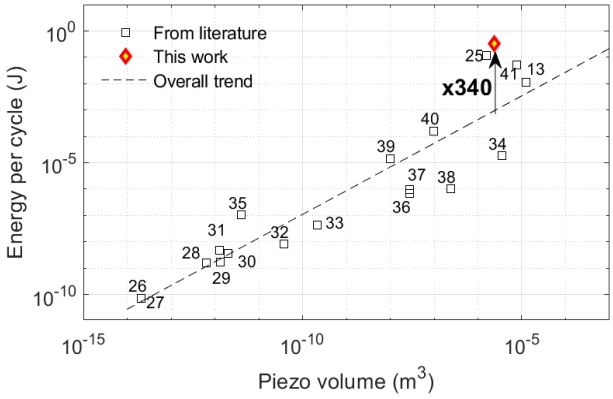

Figure 9 : General trend of the output energy of piezoelectric energy harvesting devices, as a function of the volume of the piezoelectric elements.

More generally, several works on piezoelectric energy harvesting (considering both dynamic and static regimes) were finally compared to the devices presented in this work, and listed in Table 3. It should be noted that the prototypes geometries, operating conditions, working frequency, and mechanical energy input are very different for each prototype. However, the scope of this comparison lies in the global ultimate energy harvesting capabilities, encompassing, in a pragmatic applicative way, the input mechanical energy and the part that is converted and harvested electrical. It may give an idea of the energy density of the piezoelectric materials and derive a general tendency, although each

individual point would require a specific investigation for further analysis. The output energy per cycle were plotted against the volume of the piezoelectric elements in Figure 9. The overall tendency was calculated and plotted in the figure. The different points correspond to various input mechanical energies and frequencies, so that the comparison between two points may be irrelevant. However, a global tendency arose, and it may be inferred that this comparison gives an idea of the output energy that may be reached as a function of the piezoelectric material volume. Nano and micro devices (piezo volume < 10^{-11} m^3) exhibit rather larger energy density (above the tendency) although the net output energy does not allow direct use for supplying sensors for instance, whereas millimeter to centimeter size devices (10^{-11} m^3 < piezo volume <10^{-8} m^3) are mostly below the tendency. Macroscopic devices (piezo volume >10^{-8} m^3), that include force amplification and stacked piezoelectrics, are above the tendency, thanks to a higher input mechanical energy density.

Reference	Frequency (Hz)	Volume piezo (m^3)	Output energy
Choi et al.[26]	13 970	2.12 10^{-14}	72 pJ
Jeon et al.[27]	13 900	2.12 10^{-14}	72 pJ
Muralt et al.[28]	855	6.40 10^{-13}	1.6 nJ
Shen et al.[29]	183.8	1.32 10^{-12}	1.7 nJ
Fang et al.[30]	608	1.96 10^{-12}	3.6 nJ
Shen et al.[31]	461.15	1.28 10^{-12}	4.7 nJ
Lee et al.[32]	255.9	3.75 10^{-11}	8.2 nJ
Moromoto et al.[33]	126	2.14 10^{-10}	42 nJ
Song et al. [34]	10	3.47 10^{-6}	18 µJ
Elfrink et al.[35]	572	4.04 10^{-12}	110 nJ
Ericka et al.[36]	2 580	2.82 10^{-8}	700 nJ
Minazara et al.[37]	1 710	2.82 10^{-8}	990 nJ
Chen et al.[38]	113	2.40 10^{-7}	1.0 µJ
Guyomar et al. [39]	277	1.00 10^{-8}	14 µJ
Wei et al.[40]	150	9.82 10^{-8}	163 µJ
Qian et al. [13]	1	1.27 10^{-5}	11 mJ
Wang et al.[41]	10	7.63 10^{-6}	51 mJ
Chen et al. [25]	1	1.58 10^{-6}	120 mJ
This work	**1**	**2.43 10^{-6}**	**320mJ**

Table 3 : Examples of energy harvesting prototypes, with their piezoelectric elements volume, and the output energy per cycle.

The use of Bennet's doubler in this work, that allows beneficiating of nonlinear electrical behavior, combined with the force amplification led to a much higher output energy, up to two orders of magnitude larger than the tendencies. Besides, considering that Ericsson cycles exhibited an output energy 2 to 3 times higher than Bennet's doubler interface, further gain would even be possible.

Conclusion

This work exposed a system with a mechanical amplification compressing several piezoelectric stacks, associated with a passive electrical interface able to perform large energy cycles.

Ericsson cycles were tested on two device configurations. The output energy for optimized device design #2 could reach 776 mJ (320 mJ/cm3 of piezoelectric material) per step for a force of 700 N, and an energy of 578 mJ (240 mJ/cm3) is achieved for a force of 500 N.

A model was developed for computing the mechanical input work and converted energy using idealized Ericsson cycles, allowing the assessment of the energy conversion. The analysis of this energy conversion allowed drawing insights for the development of a better configuration of piezoelectric stack assembly. Using 3 lines of 3 piezoelectric stacks and a mechanical amplification of 16, it has been possible to reach up to 1.2 J per cycle for a 500 N force application and an induced displacement of 5.7 mm. The output energy would correspond to 45% of the total stored elastic energy of 2.6 J, much higher than the 5~20% ratio experimentally usually observed in conventional devices.

As a step towards a fully functional realistic prototype, a truly passive electrical interface based on Bennet's doubler that included a storage capacitor was implemented. This led to an experimental output electrical energy of 320 mJ per cycle (130 mJ/cm3), in a truly standalone fashion.

In final experiments, the force was repeatedly applied by successive steps on the device, which could be considered as an illustration of usage for energy generation from footsteps. For a frequency of 1 Hz, this yielded an output power of 320 mW.

This unique combination between input energy optimization, transducer operating mode enhancement and electrical interface adaptation led to very high output energy, decades above the general tendency given by the literature, paving the way towards piezoelectric electrical generators featuring output energy in the Joule range for a single excitation. Such proposed prototypes may be used for example for energy harvesting in pathways from footsteps or roads.

Acknowledgements

This work was performed under the framework of the ANR-FIESTA project, funded by the French Agence Nationale pour la Recherche, grant #ANR-20-CE05-0026, and under the framework of the International Research Network ELyT Global.

References

1. Prauzek M, Konecny J, Borova M, Janosova K, Hlavica J, Musilek P. 2018 Energy Harvesting Sources, Storage Devices and System Topologies for Environmental Wireless Sensor Networks: A Review. *Sensors* **18**, 2446. (doi:10.3390/s18082446)
2. Romero E, Warrington RO, Neuman MR. 2009 Energy scavenging sources for biomedical sensors. *Physiol. Meas.*

30, R35–R62. (doi:10.1088/0967-3334/30/9/R01)
3. Stephen NG. 2006 On energy harvesting from ambient vibration. *J. Sound Vib.* **293**, 409–425. (doi:10.1016/j.jsv.2005.10.003)
4. Vocca H, Neri I, Travasso F, Gammaitoni L. 2012 Kinetic energy harvesting with bistable oscillators. *Appl. Energy* **97**, 771–776. (doi:10.1016/j.apenergy.2011.12.087)
5. Safaei M, Sodano HA, Anton SR. 2019 A review of energy harvesting using piezoelectric materials: state-of-the-art a decade later (2008–2018). *Smart Mater. Struct.* **28**, 113001. (doi:10.1088/1361-665X/ab36e4)
6. Starner T. 1996 Human-powered wearable computing. *IBM Syst. J.* **35**, 618–629. (doi:10.1147/sj.353.0618)
7. Lefeuvre E, Sebald G, Guyomar D, Lallart M, Richard C. 2009 Materials, structures and power interfaces for efficient piezoelectric energy harvesting. *J. Electroceramics* **22**, 171–179. (doi:10.1007/s10832-007-9361-6)
8. Papagiannakis AT, Dessouky S, Montoya A, Roshani H. 2016 Energy Harvesting from Roadways. *Procedia Comput. Sci.* **83**, 758–765. (doi:10.1016/j.procs.2016.04.164)
9. Chen C, Xu T-B, Yazdani A, Sun J-Q. 2021 A high density piezoelectric energy harvesting device from highway traffic — System design and road test. *Appl. Energy* **299**, 117331. (doi:10.1016/j.apenergy.2021.117331)
10. Moussa RR, Ismaeel WSE, Solban MM. 2022 Energy generation in public buildings using piezoelectric flooring tiles; A case study of a metro station. *Sustain. Cities Soc.* **77**, 103555. (doi:10.1016/j.scs.2021.103555)
11. Wen S, Xu Q, Zi B. 2018 Design of a New Piezoelectric Energy Harvester Based on Compound Two-Stage Force Amplification Frame. *IEEE Sens. J.* **18**, 3989–4000. (doi:10.1109/JSEN.2018.2820221)
12. Wang Y, Chen W, Guzman P. 2016 Piezoelectric stack energy harvesting with a force amplification frame: Modeling and experiment. *J. Intell. Mater. Syst. Struct.* **27**, 2324–2332. (doi:10.1177/1045389X16629568)
13. Qian F, Xu T-B, Zuo L. 2019 Piezoelectric energy harvesting from human walking using a two-stage amplification mechanism. *Energy* **189**, 116140. (doi:10.1016/j.energy.2019.116140)
14. Chen F, Zhang Q, Gao Y, Dong W. 2020 A Review on the Flexure-Based Displacement Amplification Mechanisms. *IEEE Access* **8**, 205919–205937. (doi:10.1109/ACCESS.2020.3037827)
15. Kim JH, Kim SH, Kwak YK. 2003 Development of a piezoelectric actuator using a three-dimensional bridge-type hinge mechanism. *Rev. Sci. Instrum.* **74**, 2918–2924. (doi:10.1063/1.1569411)
16. Ling M, Yuan L, Luo Z, Huang T, Zhang X. 2022 Enhancing Dynamic Bandwidth of Amplified Piezoelectric Actuators by a Hybrid Lever and Bridge-Type Compliant Mechanism. *Actuators* **11**, 134. (doi:10.3390/act11050134)
17. Thanh Tung N, Taxil G, Nguyen HH, Ducharne B, Lallart M, Lefeuvre E, Kuwano H, Sebald G. 2022 Ultimate electromechanical energy conversion performance and energy storage capacity of ferroelectric materials under high excitation levels. *Appl. Energy* **326**, 119984. (doi:10.1016/j.apenergy.2022.119984)
18. de Queiroz ACM, Domingues M. 2011 The Doubler of Electricity Used as Battery Charger. *IEEE Trans. Circuits Syst. II Express Briefs* **58**, 797–801. (doi:10.1109/TCSII.2011.2173963)
19. Esteves G, Fancher CM, Röhrig S, Maier GA, Jones JL, Deluca M. 2017 Electric-field-induced structural changes in multilayer piezoelectric actuators during electrical and mechanical loading. *Acta Mater.* **132**, 96–105. (doi:10.1016/j.actamat.2017.04.014)
20. Patel S, Chauhan A, Vaish R. 2014 Enhanced energy harvesting in commercial ferroelectric materials. *Mater. Res. Express* **1**, 025504. (doi:10.1088/2053-1591/1/2/025504)
21. Unruan M, Unruan S, Inkong Y, Yimnirun R. 2019 Estimation of energy density of PMN-PT ceramics utilizing mechanical stress. *Integr. Ferroelectr.* **195**, 39–45. (doi:10.1080/10584587.2019.1570042)
22. Ashley S. 2003 Artificial Muscles. *Sci. Am.* **289**, 52–59. (doi:10.1038/scientificamerican1003-52)
23. Ghaffarinejad A, Lu Y, Hinchet R, Galayko D, Hasani JY, Kim SW, Basset P. 2018 Bennet's doubler working as a power booster for triboelectric nano-generators. *Electron. Lett.* **54**, 378–379. (doi:10.1049/el.2017.3434)
24. Lefeuvre E, Risquez S, Wei J, Woytasik M, Parrain F. 2014 Self-Biased Inductor-less Interface Circuit for Electret-Free Electrostatic Energy Harvesters. *J. Phys. Conf. Ser.* **557**, 012052. (doi:10.1088/1742-6596/557/1/012052)
25. Chen C, Sharafi A, Sun J-Q. 2020 A high density piezoelectric energy harvesting device from highway traffic – Design analysis and laboratory validation. *Appl. Energy* **269**, 115073. (doi:10.1016/j.apenergy.2020.115073)
26. Choi WJ, Jeon Y, Jeong J-H, Sood R, Kim SG. 2006 Energy harvesting MEMS device based on thin film piezoelectric cantilevers. *J. Electroceramics* **17**, 543–548. (doi:10.1007/s10832-006-6287-3)
27. Jeon YB, Sood R, Jeong J -h., Kim S-G. 2005 MEMS power generator with transverse mode thin film PZT. *Sensors Actuators A Phys.* **122**, 16–22. (doi:10.1016/j.sna.2004.12.032)
28. Muralt P, Marzencki M, Belgacem B, Calame F, Basrour S. 2009 Vibration Energy Harvesting with PZT Micro Device. *Procedia Chem.* **1**, 1191–1194. (doi:10.1016/j.proche.2009.07.297)
29. Shen D, Park J-H, Noh JH, Choe S-Y, Kim S-H, Wikle HC, Kim D-J. 2009 Micromachined PZT cantilever based on SOI structure for low frequency vibration energy harvesting. *Sensors Actuators A Phys.* **154**, 103–108. (doi:10.1016/j.sna.2009.06.007)
30. Fang H-B, Liu J-Q, Xu Z-Y, Dong L, Wang L, Chen D, Cai B-C, Liu Y. 2006 Fabrication and performance of MEMS-based piezoelectric power generator for vibration energy harvesting. *Microelectronics J.* **37**, 1280–1284. (doi:10.1016/j.mejo.2006.07.023)
31. Shen D, Park J-H, Ajitsaria J, Choe S-Y, Wikle HC, Kim D-J. 2008 The design, fabrication and evaluation of a MEMS PZT cantilever with an integrated Si proof mass for vibration energy harvesting. *J. Micromechanics Microengineering* **18**, 055017. (doi:10.1088/0960-1317/18/5/055017)
32. Lee BS, Lin SC, Wu WJ, Wang XY, Chang PZ, Lee CK. 2009 Piezoelectric MEMS generators fabricated with an aerosol deposition PZT thin film. *J. Micromechanics Microengineering* **19**, 065014. (doi:10.1088/0960-1317/19/6/065014)
33. Morimoto K, Kanno I, Wasa K, Kotera H. 2010 High-efficiency piezoelectric energy harvesters of c-axis-

oriented epitaxial PZT films transferred onto stainless steel cantilevers. *Sensors Actuators A Phys.* **163**, 428–432. (doi:10.1016/j.sna.2010.06.028)
34. Song Y, Yang CH, Hong SK, Hwang SJ, Kim JH, Choi JY, Ryu SK, Sung TH. 2016 Road energy harvester designed as a macro-power source using the piezoelectric effect. *Int. J. Hydrogen Energy* **41**, 12563–12568. (doi:10.1016/j.ijhydene.2016.04.149)
35. Elfrink R, Kamel TM, Goedbloed M, Matova S, Hohlfeld D, van Andel Y, van Schaijk R. 2009 Vibration energy harvesting with aluminum nitride-based piezoelectric devices. *J. Micromechanics Microengineering* **19**, 094005. (doi:10.1088/0960-1317/19/9/094005)
36. Ericka M, Vasic D, Costa F, Poulin G, Tliba S. 2005 Energy harvesting from vibration using a piezoelectric membrane. *J. Phys. IV* **128**, 187–193. (doi:10.1051/jp4:2005128028)
37. Minazara E, Vasic D, Costa F, Poulin G. 2006 Piezoelectric diaphragm for vibration energy harvesting. *Ultrasonics* **44**, e699–e703. (doi:10.1016/j.ultras.2006.05.141)
38. Chen G, Meng Q, Fu H, Bao J. 2013 Development and experiments of a micro piezoelectric vibration energy storage device. *Mech. Syst. Signal Process.* **40**, 377–384. (doi:10.1016/j.ymssp.2013.02.009)
39. Guyomar D, Sebald G, Kuwano H. 2011 Energy Harvester of 1.5 cm3 Giving Output Power of 2.6 mW with Only 1 G Acceleration. *J. Intell. Mater. Syst. Struct.* **22**, 415–420. (doi:10.1177/1045389X10389205)
40. Wang W, Yang T, Chen X, Yao X, Qifa Zhou. 2011 Vibration energy harvesting using piezoelectric circular diaphragm array. In *2011 International Symposium on Applications of Ferroelectrics (ISAF/PFM) and 2011 International Symposium on Piezoresponse Force Microscopy and Nanoscale Phenomena in Polar Materials*, pp. 1–4. IEEE. (doi:10.1109/ISAF.2011.6014117)
41. Wang J, Cao Y, Xiang H, Zhang Z, Liang J, Li X, Ding D, Li T, Tang L. 2022 A piezoelectric smart backing ring for high-performance power generation subject to train induced steel-spring fulcrum forces. *Energy Convers. Manag.* **257**, 115442. (doi:10.1016/j.enconman.2022.115442)